LES-based prediction of technically premixed flame dynamics and comparison with perfectly premixed mode

Cite as: Phys. Fluids **34**, 085125 (2022); https://doi.org/10.1063/5.0098962
Submitted: 13 May 2022 • Accepted: 22 July 2022 • Accepted Manuscript Online: 25 July 2022 • Published Online: 17 August 2022

J. Kuhlmann, S. Marragou, I. Boxx, et al.

Physics of Fluids ARTICLE scitation.org/journal/phf

LES-based prediction of technically premixed flame dynamics and comparison with perfectly premixed mode

Cite as: Phys. Fluids **34**, 085125 (2022); doi: 10.1063/5.0098962
Submitted: 13 May 2022 · Accepted: 22 July 2022 ·
Published Online: 17 August 2022

J. Kuhlmann,[1] S. Marragou,[2] I. Boxx,[3] T. Schuller,[2] and W. Polifke[1,a)]

AFFILIATIONS

[1]Thermo-Fluid Dynamics Group, Technical University of Munich, 85747 Garching, Germany
[2]Institut de Mecanique des Fluides de Toulouse, Universite de Toulouse, CNRS, Toulouse, France
[3]Institute for Combustion Technology, German Aerospace Centre (DLR), 70569 Stuttgart, Germany

Note: This paper is part of the special topic, Development and Validation of Models for Turbulent Reacting Flows.
[a)]**Author to whom correspondence should be addressed:** polifke@tum.de

ABSTRACT

The present study combines Large Eddy Simulation (LES) with System Identification (SI) to determine the Flame Transfer Functions (FTFs) of technically premixed flames that respond to fluctuations of upstream velocity as well as equivalence ratio. Two variants to obtain the corresponding FTFs from numerically determined time series data are reported and compared with the experimental results. The experiment does not measure heat release rate directly but instead the CH^* chemiluminescence. This is insufficient for FTF identification of technically premixed flames but can be used for the validation of the simulation. We implemented a CH^* post-processor in the simulation and validated with the experiment. After validation, the simulation is used to identify the contributions of velocity and equivalence ratio to the FTF of technically premixed flame dynamics. We propose and compare two approaches for the identification of FTFs. The direct approach via multiple-input single-output system identification requires one simulation with simultaneous excitation of fuel and air inlets and carefully chosen input signals. The second approach reconstructs the FTF decomposition from two separate simulations, one perfectly premixed and one technically premixed, with reduced requirements on signal quality. We compare both approaches and discuss the FTFs of perfectly and technically premixed flames. Overall, the LES/SI approach proved to be flexible and reliable for technically premixed flames.

I. INTRODUCTION

Thermoacoustic instabilities are a major problem in almost all lean premixed or high power combustion systems, e.g., gas turbines or rocket engines.[1] Directly assessing the stability of a given system either experimentally or numerically[2] is possible but may be prohibitively expensive if several operating conditions have to be considered. The network model approach for the thermoacoustic stability analysis reduces the complexity significantly.[3] This approach requires an accurate, robust, and efficient prediction of the flame transfer function (FTF),[4] which couples acoustics with flame dynamics and vice versa.

The flame dynamics of perfectly premixed flames has been investigated extensively. The FTF can be determined by experiments[5–7] or simulations.[8,9] Experiments are expensive and time consuming to build but can produce long and extensive time series data for FTF identification. Numerical simulation, on the other hand, can be setup quickly and may even be automatized but requires significant computational resources. A multi-fidelity approach for Large Eddy Simulation (LES)/system identification (SI) can reduce return time and at the same time increase accuracy significantly.[10]

In high-power technical systems, perfect premixing cannot be achieved. Insufficient mixing and modulation of the mixing process by acoustic fluctuations cause mixture inhomogeneities, which lead to additional flame and flow perturbations.[7,11] The interference of several mechanisms of the acoustic/flow/flame interaction may provoke or dampen instability.[12,13] In order to make accurate stability predictions, all interaction mechanisms must be identified.[14]

For both experiment and simulation, the choice of the excitation scheme must be selected carefully. A high-quality signal generation is critical to correctly distinguish between the mechanisms. Experiments are often restricted due to insufficient diagnostics and construction constraints, limiting access for measurements and the excitation approach. Simulation, on the other hand, faciliates excitation of the

system in a versatile manner and optimal identification of the system dynamics. Numerical simulation depends on an adequate choice of the combustion model, turbulence model, numerical schemes, mesh base and quality, boundary conditions and much more to ensure a correct reproduction of flame dynamics.[9,15–20] Obviously, a valid estimate of the FTF can only be identified if the simulation and the identification approach are correct. It can be summarized that simulation may offer more flexibility, reliability, and shorter study durations but may be difficult to setup and, therefore, needs experiments for validation.

The PRECCINSTA gas turbine model combustor developed by Turbomeca and investigated at DLR over the past 15 years has helped deepen our understanding of the intriguing dynamics of swirling flows and swirling flames interacting with acoustic waves (see for examples Refs. 21–23). Unfortunately, until now, the flame transfer function, which describes the response of the heat release rate to acoustic perturbations, has not been characterized for this burner. Knowledge of the flame response is necessary to fully assess and interpret the combustor stability with respect to self-sustained thermoacoustic instabilities.[24–26]

The PRECCINSTA combustor can be operated in fully premixed and technically premixed (also: "partially premixed") conditions. In the latter mode of operation, the fuel is injected through small holes located within the radial swirl channel, resulting in a fuel/air mixture at the burner outlet that is not fully homogeneous. Furthermore, in the technically premixed case, acoustic oscillations in the fuel injection and mixing sections will, in general, lead to modulation of the equivalence ratio.[27] Indeed, it has been shown that self-sustained combustion oscillations in the PRECCINSTA combustor are accompanied by large fluctuations of the mixture composition at the burner outlet.[21,28]

The objective of the present study is to determine the FTF of methane/air flames in the PRECCINSTA burner. The FTF is identified not only for perfectly premixed but also for technically premixed conditions. In the experiment, the transfer function from velocity to CH^* chemiluminescence intensity is determined. These data are used to validate the numerical simulation in technically premixed conditions. The LES is used to generate multiple datasets for the identification of the velocity and equivalence ratio contribution to the FTF. Two identification approaches are tested and evaluated. The Multiple-Input, Single-Output (MISO) identification method[13,29] is tested for the first time in an LES/SI-based study of thermoacoustics.

The paper is structured as follows. Section II contains a detailed discussion of the test case, experimental setup, and simulation model and then validates the simulation results for the CH^* transfer function (CTF) against the experimental data. In Sec. III, the identification approaches are discussed and evaluated in detail.

II. EXPERIMENTAL AND NUMERICAL SETUP

The PRECCINSTA burner is a swirler-stabilized burner operating in perfectly or technically premixed conditions. When it operates in perfectly premixed conditions, the fuel-air mixture is injected at the bottom of the plenum, crosses in a radial swirler, and flows into the combustion chamber. In a technically premixed configuration, only air is injected at the bottom of the plenum, and the fuel is injected through small holes as a jet-in-cross-flow inside the swirler vane leading to partial mixing. It is operated with methane and air under atmospheric conditions. The reference case for our study has an equivalence ratio of 0.8 and a fixed thermal power of 10 kW.

A. Experiment

The original PRECCINSTA combustor has been slightly modified for the FTF measurements by replacing the bottom plate of the plenum by a transition component to fix a loudspeaker as shown in Fig. 1.

In this version, air is injected from two lateral holes at the bottom of the plenum. To allow the FTF estimation based on CH^* chemiluminescence, a photomultiplier is installed in front of the flame on one side of the transparent combustion chamber. The photomultiplier is equipped with a CH^* narrow bandpass filter (430 ± 5 nm). The reference velocity is measured in cold flow conditions (i.e., without combustion) with a hot-wire probe installed 1 mm above the injector outlet. In order to have physical access with the hot-wire probe to the outlet of the injector, a hole was drilled in one of the quartz windows of the combustion chamber. Several tests were made to determine the radial position of the hot-wire probe providing a representative signal of the oscillations of the bulk flow at the injector outlet. Experiments were only conducted for technically premixed injection conditions in which case the relationship between the CH^* flame luminosity and the heat release rate is questionable.

The CTF is determined by imposing a fixed modulation level of 15% on the flow velocity at the hot wire location when the flow is submitted to harmonic excitation with the loudspeaker,

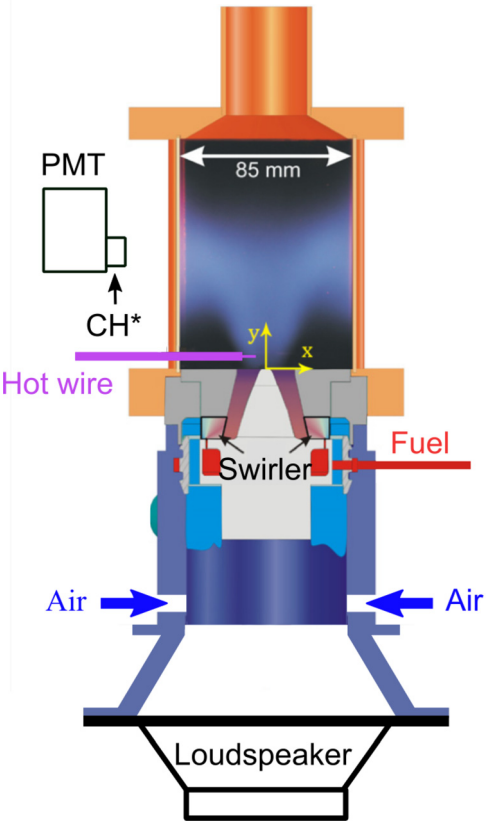

FIG. 1. Experimental sketch of the PRECCINSTA combustor with a loudspeaker at the base, a hot-wire probe, and a photomultiplier.

$$\tilde{I} = \mathcal{F}_{CH^*}\tilde{u}, \quad (1)$$

where $\tilde{I}$ and $\tilde{u}$ denote the Fourier transforms, normalized by their mean respective values, of the time series recorded by the hot wire and the photomultiplier.

Since CH^* chemiluminescence intensity depends also on the equivalence ratio, and the equivalence ratio cannot be measured with the experimental setup, the FTF cannot be reconstructed from experimental data only, and therefore, numerical simulation is needed. In order to validate the numerical results, an experimentally determined CH^* predictor is required for the simulation.

A relationship between the CH^* chemiluminescence intensity I with the thermal power $\dot{Q}$ and the equivalence ratio ϕ is adapted from Higgins *et al.*[30] and written as $I = k\dot{Q}\phi^{\beta}$, where k and β are two constants that are determined experimentally. First, the global equivalence ratio ϕ is set to 0.8, and the thermal power $\dot{Q}$ is varied. The voltage provided by the photomultiplier is plotted as a function of the thermal power $\dot{Q}$ as given in Fig. 2 (top axis). The experiments are then repeated at a thermal power fixed to 10 kW, and the equivalence ratio is varied (bottom axis).

The linearity of I with the thermal power $\dot{Q}$[31] is globally verified, and the constant k is estimated to be 0.98. The small non-linearity visible can be attributed to the effect of strain on the chemiluminescence.[32] The non-linearity of the CH^* chemiluminescence with the equivalence ratio ϕ is verified, and the exponent β is estimated to be 3.81. In both cases, the flame with a thermal power of 10 kW and a global equivalence ratio of 0.8 is considered as the reference case, and the gain of the photomultiplier was set in order to obtain a mean output voltage of $\bar{I} = 4$ V for this operating condition.

For the selected operating point of $\dot{Q} = 10$ kW and $\phi = 0.8$, the thermoacoustic state is considered to be globally stable. The Power Spectral Density (PSD) detected by the photomultiplier is plotted in Fig. 3 for cases when the loudspeaker is turned off (i.e., without external forcing) and when the loudspeaker is submitted to an harmonic excitation at 180 Hz, respectively. Although the setup is considered to be globally stable, there is some coherent activity characterized by small bumps around $f \approx 51$, 146, and 253 Hz clearly emerging from the background noise.

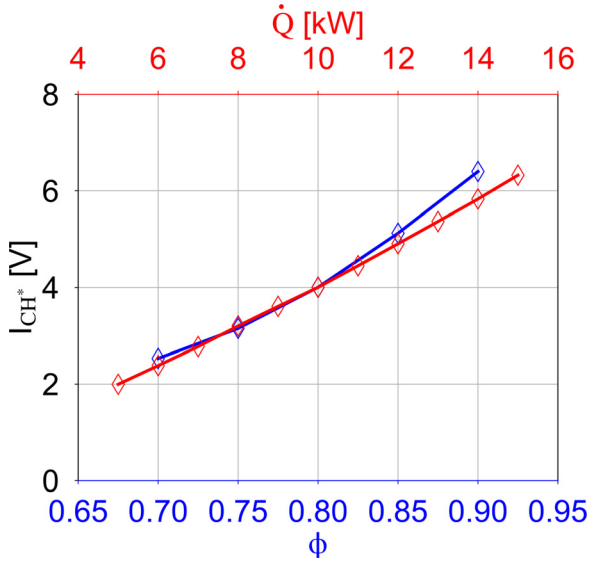

FIG. 2. CH^* chemiluminescence intensity as a function of thermal power $\dot{Q}$ for a fixed equivalence ratio $\phi = 0.8$ (top axis, red) and as a function of an equivalence ratio ϕ for fixed thermal power of 10 kW (bottom axis, blue).

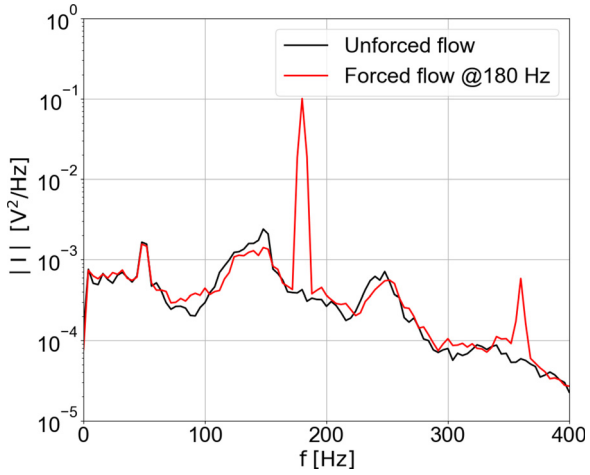

FIG. 3. Spectral Power Density (PSD) of the CH^* signal from photomultiplier in unforced and forced flow conditions.

These coherent fluctuations are naturally present without and with external forcing. They cause difficulties for transfer function determination when the flame is forced at these frequencies due to interference between the flame and flow dynamics at these naturally present frequencies and the harmonic excitation superimposed by the loudspeaker.

The coherent activity around 253 Hz is being associated with the first acoustic mode of the PRECCINSTA setup. Figure 4 shows a modal analysis of the setup using an external loudspeaker and recording of the acoustic signal inside the plenum. The signal is normalized by the pressure signal p_{ref} recorded by a microphone placed in front of the external loudspeaker. These experiments were made without combustion and without flow, and the loudspeaker at the bottom was also turned off. Acoustic modes at lower frequencies were not detected in the plenum or the combustion chamber, implying that the peaks detected at $f \approx 51$ and 146 Hz have a different origin. The tiny peak around 50 Hz may be due to an interference with the electrical network. The peak at 146 Hz may be associated with a hydrodynamic instability of the swirl flow or result from resonance with the intrinsic thermoacoustic feedback loop.

B. Numerics

We employ a generic meshing, modeling, solving, and analysis process as applied in our previous publications.[10,19] The highly automated approach allows fast adaption to new cases. The most time-consuming task is the generation of a Computer-Aided Design (CAD) model. Once this step is done, the meshing process requires just a few lines of modification in a script to adapt the refinement zones and boundary names. The boundary conditions are adapted to include separate fuel injection. The compute on a cluster, data management, and analysis are controlled by generic scripts.

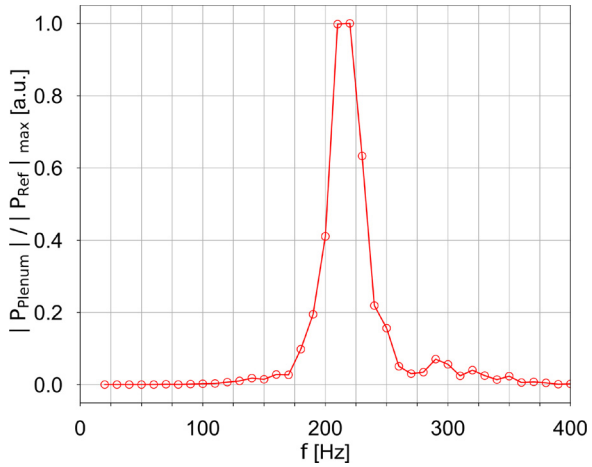

FIG. 4. Modal analysis of the plenum in cold conditions without flow.

We concentrate on a predictive evaluation and do not tune the LES. In contrast to our prior studies, the combustion model has been extended for inhomogeneous fuel–air mixtures instead of perfectly premixed gas only. The extension of the Artificial Thickened Flame (ATF) model for inhomogeneous mixture is trivial. Thanks to its generality, replacing the model constants with prior calculated functions over equivalence ratio from fully resolved laminar 1D simulations is enough.

1. Turbulent combustion LES

The pressure-based reactingFoam solver (OpenFOAM) was modified to weakly-compressible form and extended by a mixture-ratio parameterized version of the ATF model with local sensor and the BFER chemistry mechanism.[2]

The weakly-compressible formulation (ρ is only a function of T) has several advantages compared to the compressible one. It lifts the requirement of complex acoustic boundary conditions with unknown acoustic parameters, allows an increased time step size, and prevents unstable thermoacoustic modes and thereby increases signal-to-noise ratio.

In the ATF model,[33] discrete species are transported, and the reaction rates are calculated by chemistry mechanism integration. Artificial diffusivity is introduced in the flame region, which spreads the flame over a given number of cells and allows direct computation of reaction rates via the Arrhenius law. Since the thickened flame is less sensitive to wrinkling, a correction must be employed.[34] For technically premixed injection, the model parameters, laminar flame speed, the flame thickness, and flame tracking function, are functions of equivalence ratio obtained from 1D laminar fully resolved simulations. One of the biggest advantages of the model is its generality. Fuel mixtures, varying degrees of premixing, heat loss, strain, and geometric influences are directly resolved to a great extent and do not require further modeling.

The Wall-Adapting Local Eddy-viscosity (WALE) turbulence model adapts consistently toward the wall, does not require wall functions or full wall resolution, and therefore, it reduces the conditions on the mesh and allows to simplify the mesh generation process. We checked the resolution of the sub-grid scale with Pope criterion and estimation of the Taylor scale. Using the values provided by Moureau *et al.*,[35] the Taylor length scale can be estimated to be 0.7 mm for the 30 kW case. Due to the reduced Reynolds number for the 10 kW case, this value will even rise. The grid with 0.5 mm in the flame zone and further refinement at the walls and near the injectors result in the fine LES resolution.

The time step size is set at 1×10^{-6} s for the technically premixed mode, which corresponds to a maximum Courant–Friedrichs–Lewy (CFL) number of 0.4 at the injectors and typical one in the flame zone of 0.1. For the perfectly premixed mode with zero mass flow through the fuel injectors, the time step size is less restricted and can be increased to 2×10^{6} s. Actually, only a few cells at the injector edges are badly cut with a smaller volume and CFL numbers above 0.3, whereas all other cells have CFL numbers well below 0.3. This ensures correct time resolution. All equations are solved in a segregated approach with Pressure-Implicit with Splitting of Operators (PISO) pressure–velocity coupling.

Discretization schemes are all second order. We chose implicit in time (backward), central for gradients with cell-based limiter (cellLimited linear 1.0), and central gradient schemes with minimal limiting to upwind gradient in regions of highly varying gradients (limitedLinear 0.1, V for velocity, 01 for scalar, linear else) for divergence terms.

2. Boundary conditions

For this case, the swirler produces most of the turbulence, and a turbulent inflow model is not required. All walls are assumed isothermal and are set to mean values from Conjugate Heat Transfer (CHT) simulation.[36] Applying CHT would be the more robust and general approach, but we assume the heat loss modeling to be good enough considering the other uncertainties. No-slip condition is imposed at walls, and velocity signals are imposed at air and fuel inlets using "uniformFixedValue" specifying a "tableFile." The outlet imposes a total pressure and zero gradient else.

We employ broad-band signals with fixed amplitude of 15%. The broad-band excitation signal must exhibit minimal crest factor and auto-correlation, i.e., maximum amplitude utilization and signal content uniqueness, in order to investigate the system in an optimal manner and reduce required time series lengths. Furthermore, it must be smooth enough regarding the simulation time step to generate a stable and properly resolved simulation. We applied a Daubechies wavelet-based signal[37] offering the best compromise between all requirements.

3. Mesh

The mesh was built semi-automatically from a uniform background mesh and the geometry's stl file with OpenFOAM's built-in mesher snappyHexMesh. Only a few refinement regions and surfaces were specified to obtain the mesh used. Within the meshing process in snappyHexMesh, the mesh starts with a hex cell base and is refined, trimmed, and locally deformed to conform to the geometry and quality criteria. The resulting mesh may comprise arbitrary polyhedra but consists mostly of hex cells. It has around 5×10^{6} cells with a very low non-orthogonality of <45, and skewness of <2. In the flame region, the cells are of uniform size of approximately 0.5 mm, roughly equal to the flame thickness for this case, leading to a maximum thickening factor of 9. The cells close to the injector and within their jets, swirler, and bluff body walls are refined one additional level in order to accurately reproduce the geometry and the corresponding flow field.

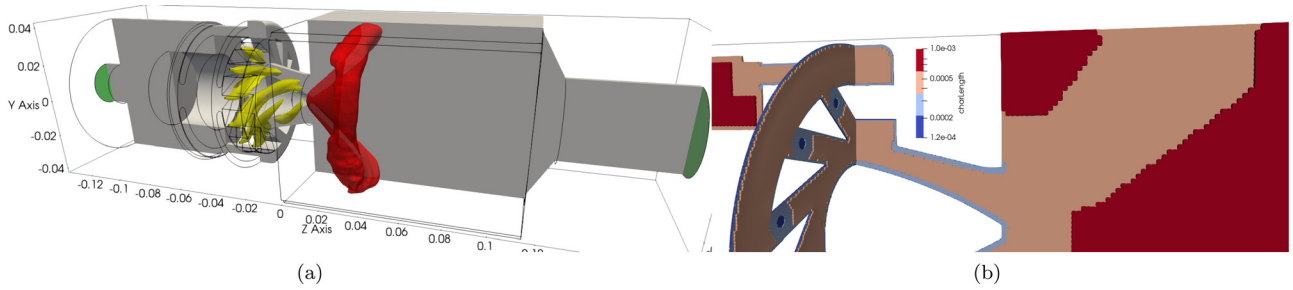

FIG. 5. Details of computational domain and mesh topology. (a) Sketch of computational domain with half cut of fluid domain and edges shown (gray), inlet and outlet boundary patches (green), and isosurfaces of mean fuel (yellow) at $\phi = 0.86$ and the mean heat release rate (red) at 10% of its maximum. (b) Mesh topology showing a cut through the swirler with the injector surface and a cut through the plenum, the swirler, the mixing tube, and the combustion chamber. Color represents refinement levels at characteristic lengths 1000, 500, 250, and 125 μm from red to blue.

Figure 5 shows a sketch of the computational domain and mesh topology. Our mesh has comparable resolution as the optimized one from Agostinelli *et al.*[38] used at the same case showing very good reproduction[36] of the experimental data. A further refinement of up to 0.25 mm in the flame zone could not improve the overall flame shape, heat release, and dynamic behavior noticeably.

4. CH* predictor

A predictor for the measured CH* is included in the simulation. It relates the local heat release rate $\dot{Q}$ and the equivalence ratio ϕ to the CH* intensity signal I as

$$I = k\dot{Q}\phi^{\beta}. \tag{2}$$

The coefficients $k = 0.98$ and $\beta = 3.81$ are determined from two steady-state experiments, one with constant power and varying mixture ratio, and vice versa, see Fig. 2. The global experimental correlations are locally applied in the LES and integrated over the volume.

C. Validation of LES

The validation process is twofold: first, we compare steady state results in terms of mean flame shape and second we compare flame dynamics in terms of FTF.

Figure 6 shows the numerically predicted mean heat release rate from our simulation with fixed temperature Boundary Condition (BC) vs the reference simulation from Agostinelli *et al.*[36] without CHT. It is important to note that our simulation employs a weakly-compressible formulation while the reference employs a fully-compressible one. The reference simulation exhibits a thermoacoustic limit cycle, which is by design not present in our simulation. The flame length and angle agree very well. The current simulation shows a more compact flame branch and higher activity towards the flame foot. This can be explained by the coarser mesh and therefore increased thickening applied in this simulation. For similar cases, a finer mesh results in an increased liftoff height and a thicker flame branch.[39] Nonetheless, the mean flame shape is qualitatively well recovered.

Since equivalence ratio measurement is unavailable in the current experiment, the FTF cannot be reconstructed, and the CTF is used for validation of the flame dynamics. We, therefore, compare the transfer functions from velocity to numerically predicted and experimentally measured CH* shown in Fig. 7.

The numerically predicted phase of the CH* transfer function—see Fig. 7 (bottom)—matches the experimentally measured one with good accuracy over the complete range of frequencies considered. The gain, on the other hand, shows discrepancies at low frequencies and in the vicinity of 260 Hz. The latter may be explained by the fact that the experiment suffers from a resonance around 260 Hz, see Fig. 4, which results in poor signal-to-noise ratio in this frequency range.

The discrepancies at low frequencies result to a certain extent from vibrations of the chamber walls, which were observed in the experiment but were of course absent in LES. More important is, however, the acoustic impedance of the fuel injection system. If a stiff injector is assumed, as set in the simulation, the low frequency limit of the CH* predictor can be approximated analytically, inspired by Polifke and Lawn.[40] In the low frequency limit and for stiff fuel injection, an increase in air mass flow rate δu results in zero change in the heat release rate $\delta\dot{Q}$. For a stiff fuel injector, equivalence ratio perturbations are directly anti-proportional to velocity perturbations at the injector:

$$\frac{\delta\phi}{\phi} = -\frac{\delta u}{u}. \tag{3}$$

The low frequency limit of the CH* predictor can be expressed as

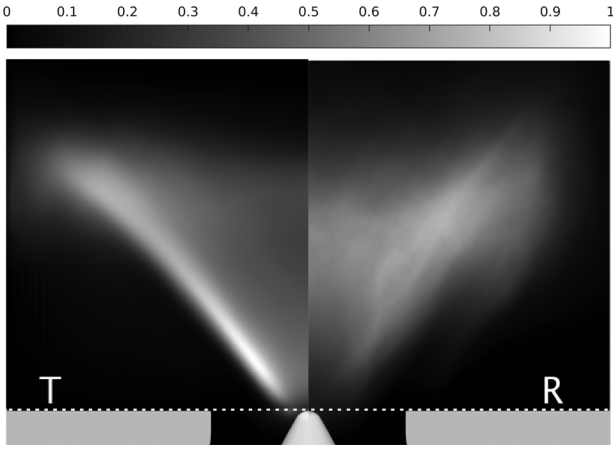

FIG. 6. Mean heat release rate for different simulations: current simulation with fixed temperature BC (T) vs reference from Agostinelli *et al.*[36] without CHT (R).

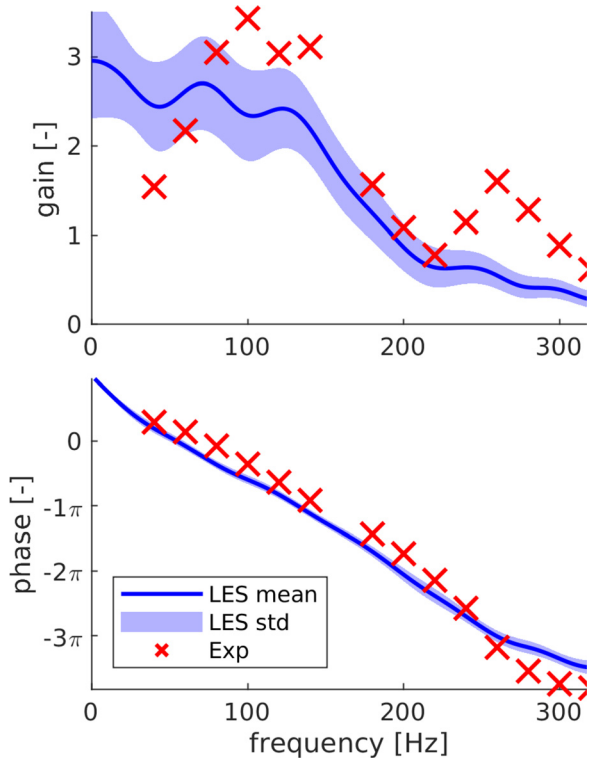

FIG. 7. CH* transfer function: experiment and LES/SI.

$$\frac{\delta I}{I} = \beta \frac{\delta \phi}{\phi} = -\beta \frac{\delta u}{u}. \tag{4}$$

In the limit of zero frequency, this gives values of $\beta = 3.81$ and π for gain and phase of the CTF, respectively. The CH* transfer function determined with LES and shown in Fig. 7 exhibits this behavior in agreement with the assumptions made.

In the experiments, on the other hand, acoustic activity has been detected in the fuel supply line during self-sustained oscillations as well as in forced flow conditions. These observations suggest that the fuel line also responds to low frequency perturbations. Assuming a quasi-steady response of the fuel line to external pressure perturbations, a link may be established between the heat release rate and CH* luminosity. A perturbation analysis yields

$$\frac{\delta \phi}{\phi} = \frac{\delta \dot{m}_f}{\dot{m}_f} - \frac{\delta \dot{m}_a}{\dot{m}_a} \approx \frac{\delta \dot{Q}}{\dot{Q}} - \frac{\delta u}{u}. \tag{5}$$

Combining this expression with Eq. (2), one obtains

$$\frac{\delta \dot{Q}}{\dot{Q}} = \frac{1}{1+\beta}\left(\frac{\delta I}{I} + \beta \frac{\delta u}{u}\right), \tag{6}$$

which accounts for the qualitative discrepancies between experimental and numerical CTF seen in Fig. 7 at low frequencies.

The origin of other discrepancies is more difficult to identify. The bump in the experimental CTF around 250 Hz could probably be attributed to the acoustic mode of the plenum at around 220 Hz. Furthermore, the loudspeaker calibration used to fix the amplitude of the velocity perturbations in the experiment was set in cold flow conditions, while the simulation used direct measurement of the velocity in hot conditions.

Taking the experimental uncertainties and the assumptions for the numerical CH* predictor into account, the agreement between numerical and experimental results is reasonable for the gain and very good for the phase. Since the numerical simulation is now verified, we want to take a closer look on the decomposition of the FTF into its contributions by velocity and equivalence ratio.

III. IDENTIFICATION APPROACH

In the perfectly premixed mode, the flame responds to velocity and swirl perturbations only. In the technically premixed mode, the flame additionally responds to equivalence ratio perturbation. This can be expressed in terms of a combined FTF.[7,13,29]

The MISO approach identifies the contributions of velocity and equivalence ratio directly from input–output data of one single simulation with simultaneous excitation of the input channels. Therein uncorrelated signals must be generated to distinguish the contributions; otherwise, the contributions may be wrongly attributed. In the experiment, the excitation of the input lines is limited. Gaseous fuel injectors may already be choked, or the equipment used for excitation may be insufficient. The generated signals are often correlated and do not satisfy the high requirements for MISO identification.

The double Single-Input, Single-Output (SISO) identification approach[7] does not require uncorrelated input channels. In fact, two separate simulations are performed, one with perfectly premixing and one with technically premixing. Their results are used to reconstruct the equivalence ratio transfer function. Therefore, the equivalence ratio must be known at the reference point, either by measurement or by transport model[41] prediction. We want to compare both identification approaches qualitatively in a numerical study.

A. Double SISO identification

In the perfectly premixed case, fuel and air mixture is injected in the air inlet only. In the technically premixed case, fuel is injected through injectors in the swirler vanes and mixed with the air cross flow. The technically premixed FTF $\mathcal{F}_{\mathrm{tp}}$ consists of velocity $\mathcal{F}_{\mathrm{u}}$ and equivalence ratio $\mathcal{F}_{\phi}$ FTFs,[13,29] with $\tilde{U}$ and $\tilde{\phi}$ being the Fourier transformed and normalized by mean velocity and equivalence ratio at the reference position, according to the following equation:

$$\mathcal{F}_{\mathrm{tp}}\tilde{U} = \mathcal{F}_{\mathrm{u}}\tilde{U} + \mathcal{F}_{\phi}\tilde{\phi}. \tag{7}$$

The underlying assumption of our decomposition approach is that we can compute the velocity FTF contribution $\mathcal{F}_{\mathrm{u}}$ of the technically premixed case from the perfectly premixed case $\mathcal{F}_{\mathrm{pp}}$. This can only hold if the flow field is similar enough and all changes in the FTFs from $\mathcal{F}_{\mathrm{tp}}$ to $\mathcal{F}_{\mathrm{pp}}$ can be attributed to the missing equivalence ratio modulation. In order to evaluate the sensitivity of $\mathcal{F}_{\mathrm{pp}}$ to changes in the flow field caused by the injector jets, we have injected perfectly premixed gas through the injectors and air inlet and investigated several injector mass flows to resemble the flow field of the technically premixed case. For our test case, the differences between zero mass flow injectors, same impulse, or same mass flow injectors were negligible due to the

small fuel injector to air inlet mass ratio. Inserting the assumption and sorting for the equivalence ratio contribution gives:[7]

$$\mathcal{F}_\phi \tilde{\phi} = (\mathcal{F}_{tp} - \mathcal{F}_{pp})\tilde{U}. \tag{8}$$

Even though we can identify both FTFs on the right-hand side from the two separate cases, both sides of the equation are referenced to different quantities $\tilde{U}$ and $\tilde{\phi}$. They must be of the same kind in order to allow computations. This can be done by inserting the velocity to equivalence ratio transfer function $\mathcal{H}$ with

$$\tilde{\phi} = \mathcal{H}\tilde{U}, \tag{9}$$

into the equation and transforming the left-hand side to $\tilde{U}$ space and solving after equivalence ratio FTF

$$\mathcal{F}_\phi = (\mathcal{F}_{tp} - \mathcal{F}_{pp})\mathcal{H}^{-1}. \tag{10}$$

The velocity to equivalence ratio transfer function is determined as input–output model from velocity and equivalence ratio signals at the reference position at the burner mouth. The choice of reference position is arbitrary but has implications on the modeling and required instrumentation. Our choice reduces the instrumentation complexity significantly but complicates the evaluation of $\mathcal{H}$. This method suffers from possible uncertainty due to the inversion and multiple identifications, i.e., amplification of their noise contributions.

Figure 8 shows the identified FTFs from technically premixed case $\mathcal{F}_{tp}$ (techPremix) and from the perfectly premixed case $\mathcal{F}_{pp}$ (fullyPremix), the velocity to equivalence ratio transfer function $\mathcal{H}$ and the reconstructed equivalence ratio contribution $\mathcal{F}_\phi$. $\mathcal{F}_{pp}$ looks as expected, i.e., it has unity gain for steady state limit, overall low-pass behavior and significant peak at lower frequencies. $\mathcal{F}_{tp}$ shows one additional peak at 140 Hz and zero gain at steady state. At steady-state velocity and equivalence ratio, contributions cancel out due to a similar gain and phase in $\mathcal{F}_u$ and $\mathcal{F}_\phi$ and a π phase delay between $\tilde{U}$ and $\tilde{\phi}$ caused by $\mathcal{H}$.

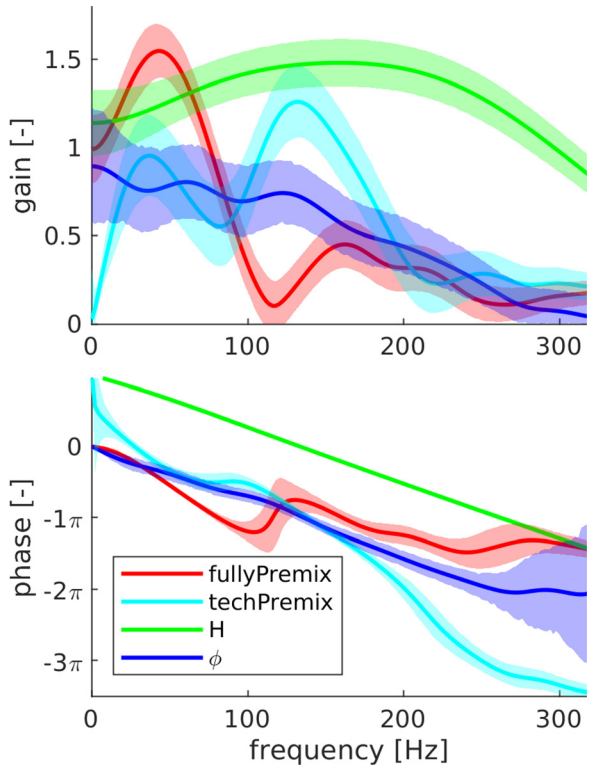

FIG. 8. Decomposed FTF from SISO LES/SI: velocity vs equivalence ratio.

$\mathcal{H}$ behavior can be explained by two major contributions; first, the mode conversion from velocity perturbations to equivalence ratio perturbations at the injectors with the constant phase delay of π and the constant gain of 1 and second, a transport part with linear phase delay and dispersive decrease in gain. The broad excess of gain around mid-frequencies can be attributed to the recirculating flow with agglomeration of fuel in the swirler vanes during the low velocity phases of the oscillations. This mechanism was observed to couple with the acoustics and cause the limit cycle oscillation.[36] The reconstructed $\mathcal{F}_\phi$ has almost unity gain for steady state limit and overall low-pass behavior without pronounced peak.

B. MISO identification

In Multiple-Input, Single-Output (MISO) identification multiple inputs are related to one output. Individual transfer functions from each input to the common output are estimated in a combined optimization process. In order to attribute the origin of a response to the correct input, the inputs must exhibit minimal cross-correlation.[42] This must be considered for the data generation process. The excitation signals must be carefully chosen for the LES to generate appropriate time series data captured at the reference point.[13,29]

In the technically premixed case of the double SISO approach, the fuel injectors were assumed to be stiff, i.e., acoustic perturbations do not alter the velocity and mass flow of the fuel injectors and mode conversion, i.e., conversion from velocity perturbations to equivalence ratio perturbations, at the injector could be assumed. The input–output data triplet with velocity and equivalence ratio as inputs and heat release rate as output was measured for the double SISO approach. Using these datasets for MISO identification do not give satisfying results, since the velocity and equivalence ratio signals at the reference position exhibit a high level of cross-correlation, making their contributions to the FTF hardly distinguishable.

Within MISO, each input channel must be excited simultaneously and independently to reduce cross-correlation significantly and allow a correct model identification. In our numerical simulation, this can be done by imposing velocity signals at the air and fuel inlets. In addition to the single broad-band signal properties, the signal pairs must exhibit minimal cross-correlation. A pair of Daubechies[37] wavelets based signals is an optimal choice.

In MISO identification, both contributions, $\mathcal{F}_u$ and $\mathcal{F}_\phi$, are directly identified. The amount of model coefficients is doubled, which may increase the required single time series length compared to SISO, but only one time series is required instead of two. The overall required time series length should be shorter for MISO.

Figure 9 shows the $\mathcal{F}_u$ and $\mathcal{F}_\phi$ from MISO identification. They look very similar to the ones obtained from double SISO approach; both satisfy the steady state limit and qualitative behavior. Only slight changes are present. Overall, the gain curves are smoother exhibiting less oscillation, and the $\mathcal{F}_\phi$ gain now shows a distinctive peak. The MISO model seems to be more reasonable but a further evaluation needs experimental reference.

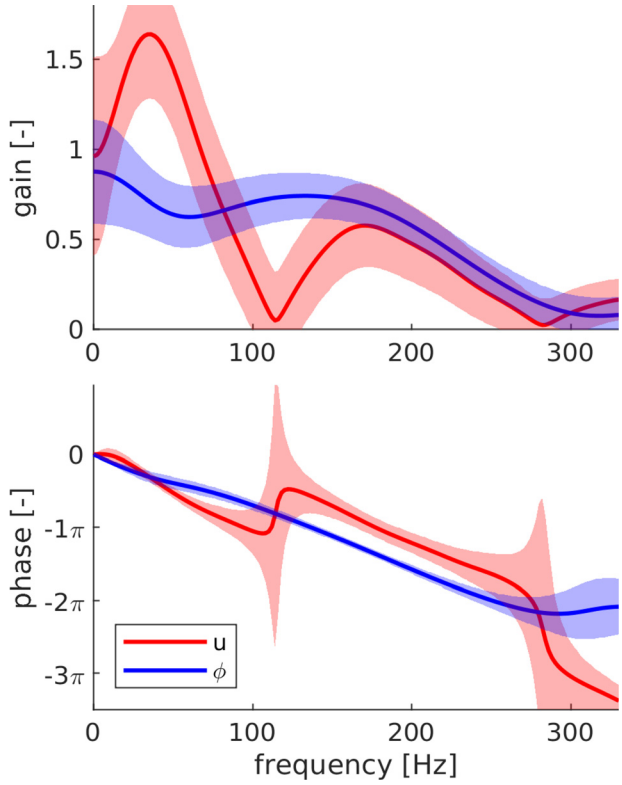

FIG. 9. FTF from MISO model identification on the heat release rate signal: velocity vs equivalence ratio.

IV. CONCLUSION

In this study, the LES/SI approach was extended and tested for a technically premixed flame test case. The straightforward computational fluid dynamics (CFD) setup approach proved to be generally applicable. In consideration of numerical model and experimental uncertainties, the LES reproduced the measurements of CH^* intensity fluctuations with very satisfactory accuracy, thereby validating the LES/SI approach.

Two variants for system identification of a technically premixed flame were tested, i.e., the double SISO and the MISO approach. Both gave comparable results for the velocity and equivalence-based FTF components. If all required data are available, the MISO identification is preferable due to a slightly better qualitative prediction of the FTFs and a reduced computational effort. The double SISO identification extends the applicability to cases, where the fuel line cannot be excited in a suitable manner. For the future, a correct modeling of the velocity-to-equivalence-ratio transfer function would allow the use of the double SISO approach in experiments, where a measurement of equivalence ratio is not possible. This would reduce the complexity and cost of experimental designs significantly.

ACKNOWLEDGMENTS

The authors gratefully acknowledge the financial support by the German Research Foundation DFG Project No. PO 710/20-1 and the provided computing time on the Leibniz Supercomputing Centres Linux-Cluster. This project has received funding from the European Research Council (ERC) under the European Union's Horizon 2020 research and innovation programme (Grant Agreement Nos. 682383 and 832248). We gratefully acknowledge that P. W. Agostinelli and T. Poinsot from CERFACS provided mean values for our thermal boundary conditions.

AUTHOR DECLARATIONS

Conflict of Interest

The authors have no conflicts to disclose.

Author Contributions

Johannes Kuhlmann: Conceptualization (lead); Data curation (lead); Investigation (lead); Methodology (lead); Software (lead); Validation (lead); Visualization (lead); Writing – original draft (lead); Writing – review and editing (lead). **Sylvain Marragou:** Investigation (supporting); Visualization (supporting); Writing – original draft (supporting); Writing – review and editing (supporting). **Isaac Boxx:** Supervision (supporting); Writing – review and editing (supporting). **Thierry Schuller:** Supervision (supporting); Writing – original draft (supporting); Writing – review and editing (supporting). **Wolfgang Polifke:** Conceptualization (supporting); Investigation (supporting); Supervision (lead); Writing – original draft (supporting); Writing – review and editing (supporting).

DATA AVAILABILITY

The data that support the findings of this study are available from the corresponding author upon reasonable request.

REFERENCES

[1]*Combustion Instabilities in Gas Turbine Engines: Operational Experience, Fundamental Mechanisms, and Modeling*, Progress in Astronautics and Aeronautics Vol. 210, edited by T. Lieuwen and V. Yang (AIAA, 2005).
[2]B. Franzelli, E. Riber, L. Y. M. Gicquel, and T. Poinsot, "Large eddy simulation of combustion instabilities in a lean partially premixed swirled flame," Combust. Flame **159**, 621–637 (2012).
[3]W. Polifke, "Low-order analysis tools for aero- and thermo-acoustic instabilities," in *Advances in Aero-Acoustics and Thermo-Acoustics*, edited by C. Schram (Von Karman Institute, Rhode-Saint-Genèse, Belgium, 2011).
[4]T. Schuller, T. Poinsot, and S. Candel, "Dynamics and control of premixed combustion systems based on flame transfer and describing functions," J. Fluid Mech. **894**, 1 (2020).
[5]P. Palies, D. Durox, T. Schuller, and S. Candel, "The combined dynamics of swirler and turbulent premixed swirling flames," Combust. Flame **157**, 1698–1717 (2010).
[6]A. Cuquel, D. Durox, and T. Schuller, "Theoretical and experimental determination of the flame transfer function of confined premixed conical flames," in 7th Mediterranean Combustion Symposium (2011).
[7]B. Cosić, S. Terhaar, J. Moeck, and C. Paschereit, "Response of a swirl-stabilized flame to simultaneous perturbations in equivalence ratio and velocity at high oscillation amplitudes," Combust. Flame **162**, 1046–1062 (2015).
[8]W. Polifke, "Black-box system identification for reduced order model construction," Ann. Nucl. Energy **67**, 109–128 (2014).
[9]X. Han, J. Li, and A. S. Morgans, "Prediction of combustion instability limit cycle oscillations by combining flame describing function simulations with a thermoacoustic network model," Combust. Flame **162**, 3632–3647 (2015).
[10]J. Kuhlmann, S. Guo, and W. Polifke, "A top level parallelization and data fusion approach for identification of flame transfer functions with increased reliability, accuracy and efficiency," in *27th International Congress on Sound*

and Vibration 2021 (ICSV27) [International Institute of Acoustics and Vibration (IIAV), 2021].
[11]T. Lieuwen and B. T. Zinn, "The role of equivalence ratio oscillations in driving combustion instabilities in low NO_x gas turbines," in *Symposium (International) on Combustion* (Elsevier, 1998), Vol. 27, pp. 1809–1816.
[12]A. Huber and W. Polifke, "Impact of fuel supply impedance on combustion stability of gas turbines," in *International Gas Turbine and Aeroengine Congress & Exposition* (ASME, 2009).
[13]A. Huber and W. Polifke, "Dynamics of practical premixed flames, part II: Identification and interpretation of CFD data," Int. J. Spray Combust. Dyn. **1**, 229–249 (2009).
[14]S. Ducruix, T. Schuller, D. Durox, and S. Candel, "Combustion dynamics and instabilities: Elementary coupling and driving mechanisms," J. Propul. Power **19**, 722–726 (2020).
[15]L. Tay-Wo-Chong, S. Bomberg, A. Ulhaq, T. Komarek, and W. Polifke, "Comparative validation study on identification of premixed flame transfer function," J. Eng. Gas Turbines Power **134**, 021502 (2012).
[16]S. Wysocki, G. Di-Chiaro, and F. Biagioli, "Effect of fuel mixture fraction and velocity perturbations on the flame transfer function of swirl stabilized flames," Combust. Theory Modell. **19**, 714–743 (2015).
[17]L. Tay-Wo-Chong, A. Scarpato, and W. Polifke, "LES combustion model with stretch and heat loss effects for prediction of premix flame characteristics and dynamics," in *ASME Turbo Expo 2017: Turbomachinery Technical Conference and Exposition* (ASME, Charlotte, NC, 2017), Vol. 4A-2017.
[18]A. Chatelier, T. Guiberti, R. Mercier, N. Bertier, B. Fiorina, and T. Schuller, "Experimental and numerical investigation of the response of a swirled flame to flow modulations in a non-adiabatic combustor," Flow, Turbul. Combust. **102**, 995–1023 (2019).
[19]J. Kuhlmann, A. Lampmann, M. Pfitzner, and W. Polifke, "Assessing accuracy, reliability and efficiency of combustion models for prediction of flame dynamics with large eddy simulation," Phys. Fluids (published online, 2022).
[20]F. Dupuy, M. Gatti, C. Mirat, L. Gicquel, F. Nicoud, and T. Schuller, "Combining analytical models and les data to determine the transfer function from swirled premixed flames," Combust. Flame **217**, 222–236 (2020).
[21]W. Meier, P. Weigand, X. R. Duan, and R. Giezendanner-Thoben, "Detailed characterization of the dynamics of thermoacoustic pulsations in a lean premixed swirl flame," Combust. Flame **150**, 2–26 (2007).
[22]A. M. Steinberg, I. Boxx, M. Stöhr, C. D. Carter, and W. Meier, "Flow–flame interactions causing acoustically coupled heat release fluctuations in a thermoacoustically unstable gas turbine model combustor," Combust. Flame **157**, 2250–2266 (2010).
[23]I. Boxx, M. Stoehr, W. Meier, and C. Carter, "Temporally resolved planar measurements of transient phenomena in a partially pre-mixed swirl flame in a gas turbine model combustor," Combust. Flame **157**, 1510 (2010).
[24]A. P. Dowling and S. R. Stow, "Acoustic analysis of gas turbine combustors," J. Propul. Power **19**, 751–764 (2003).
[25]T. Sattelmayer and W. Polifke, "Assessment of methods for the computation of the linear stability of combustors," Combust. Sci. Technol. **175**, 453–476 (2003).
[26]T. Poinsot, "Prediction and control of combustion instabilities in real engines," Proc. Combust. Inst. **36**, 1–28 (2017).
[27]P. W. Agostinelli, D. Laera, I. Chterev, I. Boxx, L. Gicquel, and T. Poinsot, "On the impact of H_2-enrichment on flame structure and combustion dynamics of a lean partially-premixed turbulent swirling flame," Combust. Flame **241**, 112120 (2022).
[28]M. Stoehr, Z. Yin, and W. Meier, "Interaction between velocity fluctuations and equivalence ratio fluctuations during thermoacoustic oscillations in a partially premixed swirl combustor," Proc. Combust. Inst. **36**, 3907–3915 (2017).
[29]A. Huber and W. Polifke, "Dynamics of practical premixed flames, part I: Model structure and identification," Int. J. Spray Combust. Dyn. **1**, 199–228 (2009).
[30]B. Higgins, M. McQuay, F. Lacas, and S. Candel, "An experimental study on the effect of pressure and strain rate on CH chemiluminescence of premixed fuel-lean methane/air flames," Fuel **80**, 1583–1591 (2001).
[31]I. R. Hurle, R. B. Price, T. M. Sugden, and A. Thomas, "Sound emission from open turbulent premixed flames," Proc. R. Soc. London, Ser. A **303**, 409–427 (1968).
[32]V. N. Nori and J. M. Seitzman, "CH^* chemiluminescence modeling for combustion diagnostics," Proc. Combust. Inst. **32**, 895–903 (2009).
[33]O. Colin, D. F, V. D, and T. Poinsot, "A thickened flame model for large eddy simulations of turbulent premixed combustion," Phys. Fluids **12**(7), 1843 (2000).
[34]F. Charlette, C. Meneveau, and D. Veynante, "A power-law flame wrinkling model for les of premixed turbulent combustion part I: Non-dynamic formulation and initial tests," Combust. Flame **131**, 159–180 (2002).
[35]V. Moureau, P. Domingo, and L. Vervisch, "From large-eddy simulation to direct numerical simulation of a lean premixed swirl flame: Filtered laminar flame-PDF modeling," Combust. Flame **158**, 1340–1357 (2011).
[36]P. W. Agostinelli, D. Laera, I. Boxx, L. Gicquel, and T. Poinsot, "Impact of wall heat transfer in large eddy simulation of flame dynamics in a swirled combustion chamber," Combust. Flame **234**, 111728 (2021).
[37]S. Föller and W. Polifke, "Advances in identification techniques for aeroacoustic scattering coefficients from large eddy simulation," in *18th International Congress on Sound and Vibration (ICSV18)* (International Institute of Acoustics and Vibration, Rio de Janeiro, Brazil, 2011), Vol. 4.
[38]P. W. Agostinelli, B. Rochette, D. Laera, J. Dombard, B. Cuenot, and L. Gicquel, "Static mesh adaptation for reliable large eddy simulation of turbulent reacting flows," Phys. Fluids **33**, 035141 (2021).
[39]P. Benard, G. Lartigue, V. Moureau, and R. Mercier, "Large-eddy simulation of the lean-premixed PRECCINSTA burner with wall heat loss," Proc. Combust. Inst. **37**, 5233–5243 (2019).
[40]W. Polifke and C. Lawn, "On the low-frequency limit of flame transfer functions," Combust. Flame **151**, 437–451 (2007).
[41]V. Kather, F. Lückoff, C. Paschereit, and K. Oberleithner, "Interaction of equivalence ratio fluctuations and flow fluctuations in acoustically forced swirl flames," Int. J. Spray Combust. Dyn. **13**, 72 (2021).
[42]A. Tangirala, *Principles of System Identification: Theory and Practice* (CRC Press, 2018).